Bioactive Materials 7 (2022) 3–13

Contents lists available at ScienceDirect

Bioactive Materials

journal homepage: www.sciencedirect.com/journal/bioactive-materials

Porous tantalum structure integrated on Ti6Al4V base by Laser Powder Bed Fusion for enhanced bony-ingrowth implants: In vitro and in vivo validation

Pengfei Lei [a,b,c,1], Hu Qian [a,1], Taomei Zhang [c], Ting Lei [a], Yihe Hu [a,b,*], Chao Chen [a,c,**], Kechao Zhou [c]

[a] Department of Orthopedic Surgery, Hunan Engineering Research Center of Biomedical Metal and Ceramic Implants, Xiangya Hospital, Central South University, Changsha 410008, China
[b] Department of Orthopedic Surgery, The First Affiliated Hospital, College of Medicine, Zhejiang University, China
[c] State Key Laboratory of Powder Metallurgy, Central South University, Changsha, 410083, China

ARTICLE INFO

Keywords:
Tantalum
Ti6Al4V
Laser powder bed fusion
Orthopedic scaffolds
Osteointegration

ABSTRACT

Despite the widespread application of Ti6Al4V and tantalum (Ta) in orthopedics, bioinertia and high cost limit their further applicability, respectively, and tremendous efforts have been made on the Ti6Al4V-Ta alloy and Ta coating to address these drawbacks. However, the scaffolds obtained are unsatisfactory. In this study, novel high-interface-strength Ti6Al4V-based porous Ta scaffolds were successfully manufactured using Laser Powder Bed Fusion for the first time, in which porous Ta was directly manufactured on a solid Ti6Al4V substrate. Mechanical testing revealed that the novel scaffolds were biomechanically compatible, and the interfacial bonding strength was as high as 447.5 MPa. In vitro biocompatibility assay, using rat bone marrow mesenchymal stem cells (r-BMSCs), indicated that the novel scaffolds were biocompatible. Alkaline phosphatase and mineralized nodule determination demonstrated that the scaffolds favored the osteogenic differentiation of r-BMSCs. Moreover, scaffolds were implanted into rabbits with femur bone defects, and imaging and histological evaluation identified considerable new bone formation and bone ingrowth, suggesting that the scaffolds were well integrated with the host bone. Overall, these results demonstrated good mechanical compatibility, biocompatibility, and osteointegration performance of the novel Ti6Al4V-based porous Ta scaffold, which possesses great potential for orthopedic clinical applications.

1. Introduction

The application of metallic biomaterials to load-bearing orthopedic implants has attracted extensive attention in recent decades [1]. Ti6Al4V is the most common titanium alloy used in orthopedics because of its excellent corrosion resistance and biomechanical properties [2,3]. However, the osteointegration of Ti6Al4V is not satisfactory because of its bioinert property and high elasticity, which may impede early bone-implant fixation and long-term stability, leading to aseptic loosening and presenting an obstacle for its widespread application [4]. Tantalum (Ta) is also widely used in orthopedics. Ta is a bioactive metal with outstanding osteogenic properties and excellent biocompatibility and has gained increasing attention in recent years [4,5]. In particular, since the introduction of the Trabecular Metal (Zimmer Biomet), the clinical application of Ta has increased boomingly [6]. Although clinical and laboratory studies have demonstrated the osteointegration of Ta, its widespread applicability is limited by the relatively high cost of processing and high density [7].

Considering the complementary merits of Ti6Al4V and Ta, great efforts have been made to fabricate Ti6Al4V (Ti)/Ta composite scaffolds; alloying and coating are the two most popular approaches [4,7–13]. However, inevitable shortcomings still exist in both approaches,

Peer review under responsibility of KeAi Communications Co., Ltd.
* Corresponding author. Department of Orthopedic Surgery, Xiangya Hospital Central South University, Changsha, 410008, China.
** Corresponding author. State Key Laboratory of Powder Metallurgy, Central South University, Changsha, 410083, China.
E-mail addresses: pengfeilei@csu.edu.cn (P. Lei), moneylakecsu@163.com (H. Qian), csuhuyihe@163.com (Y. Hu), pkhqchenchao@126.com (C. Chen).
[1] These authors contributed equally to this work.

https://doi.org/10.1016/j.bioactmat.2021.05.025
Received 22 March 2021; Received in revised form 11 May 2021; Accepted 14 May 2021
Available online 16 June 2021

including unfavorable biomechanical properties, non-optimized alloying ratio, undesirable bioactivity, and non-porous structure [7–11,13].

Therefore, the development of Ti6Al4V/Ta composite scaffolds would make great sense. The drawbacks derived from the two metals could be overcome, and the excellent mechanical properties of Ti6Al4V and the considerable osteointegration of Ta could be combined. However, the fabrication of such scaffolds is difficult because the melting point of Ta is as high as 3017 °C, and it is highly affiliative to oxygen [7]. Fortunately, additive manufacturing (AM, also known as 3D printing), which enabled great breakthroughs in the fabrication of orthopedic implants [14–16], also enables the successful fabrication of such metallic scaffolds. Moreover, AM addresses some potential shortcomings of scaffolds manufactured using conventional methods, such as undesirable mechanical properties and inhomogeneous pore size [17]. In particular, it has been deemed feasible to modify the geometry, pore size, and architectural characteristics of Ti6Al4V using Laser Powder Bed Fusion (LPBF) without varying the mechanical properties remarkably [18], implying that devices manufactured using AM could be optimized by tailoring the properties.

In this study, we developed a novel high-interface-strength Ti6Al4V-based porous Ta scaffold using LPBF, a type of AM technology [19], in which the Ti6Al4V substrate was manufactured first and porous Ta was fabricated on it directly. Through this approach, the porous Ta structure and solid Ti6Al4V was combined metallically. The mechanical properties and bonding strength of the novel scaffold were determined via mechanical testing. Thereafter, the biological performance, including cellular adhesion, cellular morphology, cellular proliferation, and osteointegration, were also evaluated via in vitro and in vivo experiments.

To the best of our knowledge, the present study is the first to report a high-interface-strength Ti6Al4V-based porous Ta scaffold fabricated through AM, which possesses great potential for clinical translation. Our work may provide innovative insights and inspiration for the design and development of clinical orthopedic implants.

2. Materials and methods

2.1. Fabrication of the novel scaffolds

Three groups of Ti6Al4V-based porous Ta scaffolds, namely group A, B, and C, were manufactured using an LPBF system (FS271 M Farsoon, China). Strut sizes, porosities, and pore sizes of the three groups are listed in Table 1. According to previous study, we selected diamond lattice structure in the designing of porous Ta scaffolds [20]. Briefly, a solid column structure was designed on the solid disc structure, and then the diamond crystal lattice (Fig. 1a) structure was imported into the column, which was saved in the form of an STL file. Then, a computer-aided design (CAD) model was generated based on the STL file using CAD software, which was imported into the LPBF printer. The diameter of the spherical Ta powder was in the range of 10–40 μm (Fig. 1b), and the mean diameter of the spherical Ti6Al4V powder was 38.05 μm (Fig. 1c). When the previously treated Ta powder or Ti6Al4V powder was melted using the laser and consolidated, another layer of powder was deposited on the former layer immediately until the scaffolds were fully fabricated in the manufacturing chamber (Fig. 1d). After the solid Ti6Al4V substrate was formed, Ta powder was deposited onto the substrate successively, and the porous Ta scaffold was manufactured layer by layer. The entire manufacturing process was conducted under an argon atmosphere. The specific processing parameter for Ta was a laser with a power of 300W and a scanning speed of 250 mm/s, while for Ti6Al4V it was a laser with a power of 250 W and a scanning speed of 300 mm/s. The scaffolds used for both in vitro and in vivo experiments were Ø 4.5 mm × 5 mm, the substrate of which was 2 mm thick and the porous section was 3 mm. After manufacturing, the samples used for testing interfacial bonding strength were sliced into flat dog-bone-shaped coupons. All the samples were treated with annealing at 1000 °C under a vacuum environment for 30 min. The lost and semi-lost powders were removed using air gun blowing, and ultrasonic cleaning with absolute ethyl alcohol, acetone and double distilled H_2O for 15 min in sequence.

Table 1
Morphological properties of the novel scaffolds.

Groups	Group A	Group B	Group C
Pore structure	diamond	diamond	diamond
Struct size (mm)			
Designed	0.212	0.391	0.495
Manufactured	0.191	0.323	0.435
Pore size (mm)			
Designed	0.462	0.685	0.894
Manufactured	0.413	0.622	0.830
Porosity (%)			
Designed	70	70	70
Manufactured	72.1	71.9	71.1

2.2. Sample characterization

Surface topography and microstructure of scaffolds in different groups were visualized using scanning electron microscopy (SEM, TESCAN, USA). The actual strut size and pore size were measured based on SEM results, and the actual porosity was determined using an automatic density analyzer (Quantachrome, USA). The distribution of elements on the surface of the scaffolds and the interface between the Ti6Al4V substrate and porous Ta was detected using energy-dispersive spectrometry (EDS, TESCAN, China).

2.3. Mechanical testing

Mechanical tests were conducted using a mechanical testing machine (Instron 3369, America). Following the ASTM E9-09 standard (2018), six cylindrical scaffolds (Ø 10 mm × 25 mm) Ta scaffolds were manufactured for the detection of compressive strength and modulus in each group. Six solid flat dog-bone-shaped coupons with a gauge length of 25 mm were fabricated for testing the interfacial bonding strength.

2.4. Cellular experiments

2.4.1. Isolation and culturing of BMSC

Rat bone marrow mesenchymal stem cells (r-BMSCs) were isolated according to a standard protocol described previously [21]. In brief, femurs and tibias were extracted from Sprague Dawley rats weighing 60–80 g, and the attached soft tissues were removed completely. The fresh bone marrow was then blown out with a 1 mL syringe and cultured in Dulbecco's modified Eagle medium (DMEM)/F12 (Gibco, USA) supplemented with fetal bovine serum (FBS, 10%, Thermo, China) and penicillin-streptomycin (1%, HyClone, China) at 37 °C and 5% CO_2 concentration. Half of the medium was changed every day and fully renewed every two days after culturing for 96 h. r-BMSCs were used for subsequent experiments at the third passage.

2.4.2. Cellular morphology and proliferation

r-BMSCs were seeded onto the Ti6Al4V-based porous Ta scaffolds in different groups, and phalloidin (Thermo, China)/4',6-diamidino-2-phenylindole (DAPI, GENVIEW, China) staining and SEM were performed to evaluate cellular morphology. Cell counting Kit-8 (CCK-8, Dojindo, Japan) was used to detect the proliferation of r-BMSCs.

For SEM characterization, 5×10^3 r-BMSCs were seeded onto the surface of the scaffolds in different groups in 96-well plates and cultured as described above. After 2- and 12-days of culture, the scaffolds were washed with phosphate-buffered saline (PBS) twice and treated with paraformaldehyde (PFA) at 4 °C for over 4 h, and then dehydrated with alcohol gradient. Finally, a layer of gold was deposited onto the surface

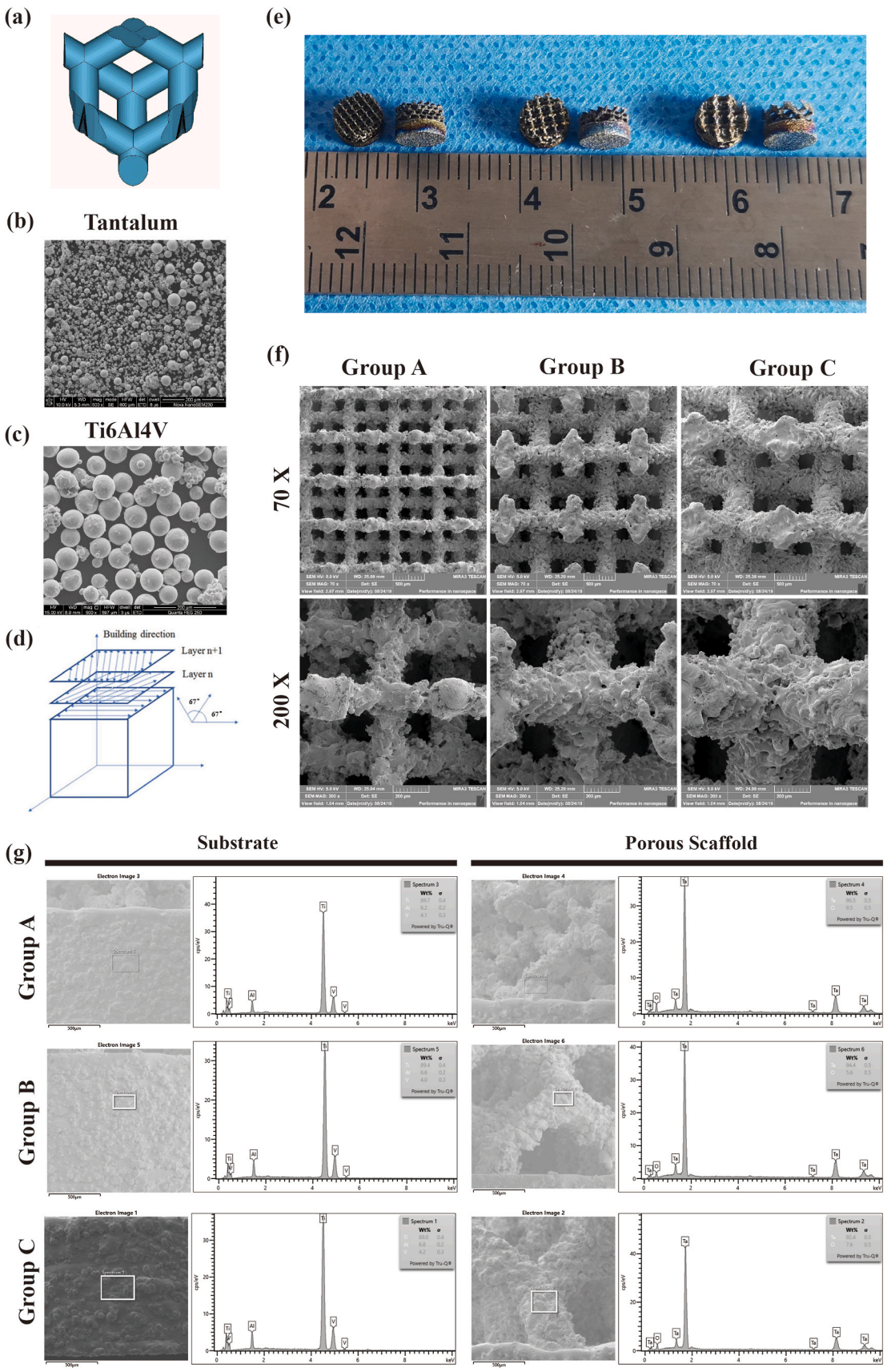

Fig. 1. Fabrication and characterization of the novel scaffolds. (a) 3-dimensional view of the diamond unit cell, (b) spherical tantalum and Ti6Al4V powders used for the fabrication of the novel scaffolds, (d) building orientation of the samples, (e) overview of the manufactured samples, (f) scanning electron microscopy (SEM) images of the samples, (g) representative images of Energy-Dispersive Spectrometry (EDS) detection for the samples.

of the scaffolds, and the cellular morphology was observed using SEM (TESCAN, USA).

For phalloidin/DAPI staining, 5×10^3 r-BMSCs were seeded on the scaffolds in 96-well plates, and the medium was replaced every two days. After culturing with DMEM/F12 supplemented with 10% FBS at 37 °C and 5% CO_2 for 7 days, the scaffolds were washed twice with PBS (GENVIEW, China) and fixed with 4% PFA at 25 °C for 30 min. Next, the scaffolds were treated with 0.1% Triton X-100 for 10 min to perforate the cytomembrane. Then, phalloidin and DAPI solution were added to stain the cytoskeleton and nucleus, and images were captured using a laser confocal microscope (TCP SP8 X, Leica, Germany) [22].

For the CCK8 assay, 1×10^4 r-BMSCs were seeded onto the scaffolds in different groups in 96-well plates, and equivalent cells were seeded in the blank well, which was set as the control group. r-BMSCs were cultured with DMEM/F12 supplemented with 10% FBS, and the medium was replaced every two days. On days 1, 3,5, and 7, the cells were incubated with the CCK8 reagent diluted in the medium at a ratio of 1:10 for 1.5 h, and 100 μL supernatant was collected to detect the optical density (OD) using a microplate reader (M200PRO, Tecan, Switzerland) at 450 nm.

2.4.3. Osteogenic differentiation evaluation

Alkaline phosphatase (ALP) production was detected using an ALP kit (Jiancheng, China). In brief, 2×10^4 r-BMSCs were seeded onto the scaffolds in 96-well plates, and the medium was replaced with osteogenic medium (α-MEM medium (Thermo, China) supplemented with 10% FBS, 1% penicillin-streptomycin, 1 mM dexamethasone, 1 M β glycerol phosphate, and 10 mM ascorbic acid) on the second day. After culturing with the osteogenic medium for 3 and 7 days, 5 μL of the supernatant was transferred into a complex solution containing 50 μL substrate and 50 μL buffer in a 96-well plate and incubated at 37 °C for 20 min. A color agent (150 μL) was added to each well, and the OD value was measured at 520 nm using a microplate reader.

For mineralized nodule staining and semi-quantification, r-BMSCs (2×10^4) were seeded onto the scaffolds in 96-well plates and cultured in an osteogenic medium for 14 days. After washing with PBS two times and fixing with PFA at 25 °C for 30 s, alizarin red solution was added to the plate to stain the mineralized nodules, and then images were captured using a light microscope. After imaging, scaffolds were washed with PBS until the solution became clear, and cetylpyridinium chloride (10%, Sigma, USA) was added to the plates to degrade the stained mineralized nodules. Exactly 100 μL of the dissolved solution was collected to detect the OD at 562 nm.

2.5. Animal experiments

2.5.1. Construction of the bone defect model

All animal experiments in the present study were approved by the Animal Ethics Committee of Xiangya Hospital (No: 2019sydw0126). Thirty 10-week old New Zealand rabbits weighing 2 kg (male) were randomly allocated to three groups. All rabbits were anesthetized with 0.1% sodium pentobarbital. Shaving, disinfection, and the sterile sheet covering were performed strictly according to sterility principles. To expose the lateral femoral condyle, a 2 cm incision was made on the lateral side of the distal femur, and the soft tissue and muscle covering the lateral femoral condyle were bluntly separated. A cylindrical bone defect of Ø4.5 × 5 mm was prepared using an electric drill, which was perpendicular to the surface of the lateral femoral condyle. Scaffolds from different groups were implanted into the defects, with the porous Ta inside, and the Ti6Al4V substrate was outside. After surgery, the incision was sutured layer by layer, and each rabbit was injected with 40,000 U penicillin.

2.5.2. Imageology evaluation

Six weeks after implantation, animals were sacrificed via overdose sodium pentobarbital injection. After the soft tissue was removed, the femurs were collected and fixed in 4% PFA for several days. X-ray images of the femur specimens were photographed using a C-arm machine (Vetoo, 200 A). The bone remodeling related parameters, including trabecular number (Tb·N) and the ratio of bone volume to tissue volume (BV/TV), were detected using a micro-CT machine (Skyscan 1172, Belgium).

2.5.3. Histological analysis

After imaging, the samples were prepared for histological analysis. First, the lateral femoral condyle samples were immersed in a 10% formaldehyde solution for 1 d and dehydrated in alcohol gradient. The dehydrated samples were embedded in 15.7% methyl methacrylate (MMA) for 4 h. Thereafter, the samples were prepared using a hard tissue slicer (Eckart 300, Germany) [23]. For the staining, van Geison's picrofuchsin and toluidine blue were applied to stain the prepared hard tissue sections [17], and the stained samples were imaged using an optical microscope (Leica, Germany). Furthermore, hard tissue sections were prepared for SEM and to explore the distribution of elements using EDS.

2.6. Statistical analysis

Statistical analysis was performed using SPSS software (version 14.0, Chicago, USA). The results were presented as the mean ± standard deviation. The student's 2-tailed *t*-test was selected for the statistical comparison between two groups, and a one-way ANOVA test was chosen for the statistical comparison of results among three or more groups. When a p-value of <0.05 was identified using a one-way ANOVA test, a q test was applied among multiple groups. Statistical significance was set at $p < 0.05$.

3. Results

3.1. Scaffolds characterization

3.1.1. Morphological characteristics and EDS results

Ti6Al4V-based porous Ta scaffolds were successfully fabricated using LPBF (Fig. 1e). The top view of the scaffolds at different magnifications was captured using SEM, which showed uniformly distributed porous structures and homogeneous pore sizes in each group (Fig. 1f). The actual porosities of groups A, B, and C were 72.1, 71.9, and 71.1%, respectively, and the actual pore sizes ranged from 0.413 to 0.830 mm (Table 1). EDS confirmed that the substrate was made up of Ti6Al4V, while the porous scaffolds were made from Ta (Fig. 1g).

3.1.2. Mechanical properties

A compression test was performed to assess the mechanical properties of the different groups of scaffolds. The representative stress-strain curves generated from the compression test are shown in Fig. 2a, and the specific compressive modulus and compressive strength are summarized in Table 2. The mean compressive moduli of groups A, B, and C were 0.58, 1.47, and 1.51 GPa, respectively, all of which were in the range of the compressive modulus of human bone tissue (0.5–20 GPa) [17], and lower than previous reports [17,24]. The average compressive strengths of groups A, B, and C were 6.812, 12.321, and 27.852 MPa, respectively. These results revealed that the mechanical properties of the newly developed scaffolds were suitable for orthopedic implantation.

3.1.3. Interfacial bonding strength

Next, the interfacial bonding strength between the Ti6Al4V and Ta was detected using a tensile test (Fig. 2c and d). One side of the flat dog-bone-shaped coupons was made of Ta, and another side was made of Ti6Al4V (Fig. 2c). The representative stress-strain curve is depicted in Fig. 2e. The mean ultimate interfacial bonding strength was as high as 447.5 MPa, which was nearly ten times that of human femoral cortical bone [25]. To further explore the binding strength between the substrate

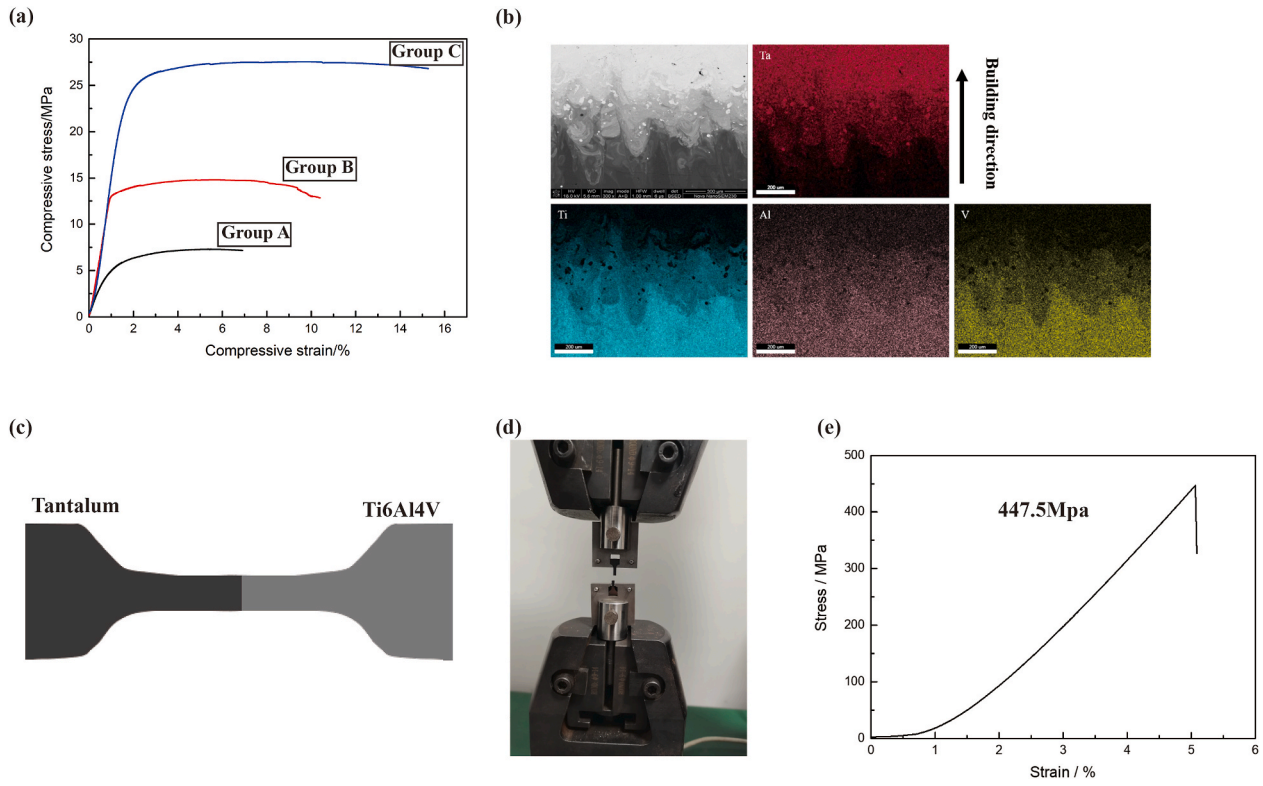

Fig. 2. Mechanical testing of the novel scaffolds. (a) Representative strain-stress curve of the compressive test, (b) distribution images of elements in the interface detected using Energy-Dispersive Spectrometry (EDS), (c) schematic diagram of the flat dog-bone-shaped coupons, (d) tensile test, (e) representative strain-stress curve of the tensile test.

Table 2
Mechanical properties of the novel scaffolds.

Groups	Group A	Group B	Group C
Elasticity modulus (GPa)	0.58	1.47	1.51
Compressive strength (MPa)	6.812	12.321	27.852

and the porous Ta, the distribution of elements in the interface was determined. As shown in Fig. 2b, the porous Ta and the substrate Ti6Al4V infiltrated the interface locally, resulting in a locally diffused alloy-like interface, which may contribute to the increased binding strength at the interface. These results demonstrate that the substrate Ti6Al4V and porous Ta were tightly bonded, which is sufficient for orthopedic implants.

3.2. In vitro biocompatibility

3.2.1. Cell morphology

The morphology of r-BMSCs on the three groups of scaffolds was visualized using SEM and a laser confocal microscope. SEM images showed that r-BMSCs adhered freely on the top of the porous scaffolds after 2 days and exhibited extending pseudopods preliminarily in all three groups (Fig. 3a). After 12 days, significant morphological changes and increased amounts of r-BMSCs were observed, with more and longer cellular pseudopods connected to form a film layer, which covered the surfaces of the porous scaffolds. In line with the SEM results, confocal images revealed that after culturing for 7 days, r-BMSCs in all three groups spread out fully and connected with adjoining cells via affluent filopodia to form a complex network structure (Fig. 3b). The signal intensity ratio of phalloidin-labeled cell cytoskeleton (green) to DAPI-labeled nucleus (blue) was as high as 3.57–11.86 (Fig. 3c).

3.2.2. Cell proliferation

Proliferation was tested using the CCK8 assay over a culturing period of 7 days. As illustrated in Fig. 3d, a stable proliferation was observed in all groups as the culture time increased. No significant difference was observed between the control group and all three experimental groups on days 1 and 3. Meanwhile, the proliferation of cells in group C scaffold remained comparable to that of the control group on days 5 and 7.

These results synergistically revealed that the biocompatibility of the Ti6Al4V-based porous Ta scaffolds was excellent.

3.3. In vitro osteogenic property

The production of ALP was detected over a culturing period of 7 days. There was a notable increase from days 3–7 (Fig. 4a). Statistic differences were identified among the three groups at both time points, and group C scaffolds showed the highest value. The mineralization capacity of r-BMSCs on the surface of the porous scaffolds was evaluated via alizarin red staining and the corresponding semi-quantitative analysis after culturing for 14 days. As depicted in Fig. 4b, considerable mineralized nodules were observed in each group. The semi-quantitative analysis after dissolution showed that the OD ranged from 1.56 to 2.06, which indicated the excellent mineralization capacity of the scaffolds. These findings suggested that the Ti6Al4V-based porous Ta scaffolds possessed excellent osteogenic capabilities (Fig. 4c).

3.4. In vivo osteointegration property

3.4.1. Radiologic evaluation

After implantation for 6 weeks, X-ray and micro-CT were applied to evaluate osteointegration. In X-ray images, the Ti6Al4V-based porous Ta scaffolds were well implanted into the distal femur completely, and no dislocation of the scaffolds, periprosthetic osteolysis or fracture was observed. The new bone not only grew around the scaffolds but also

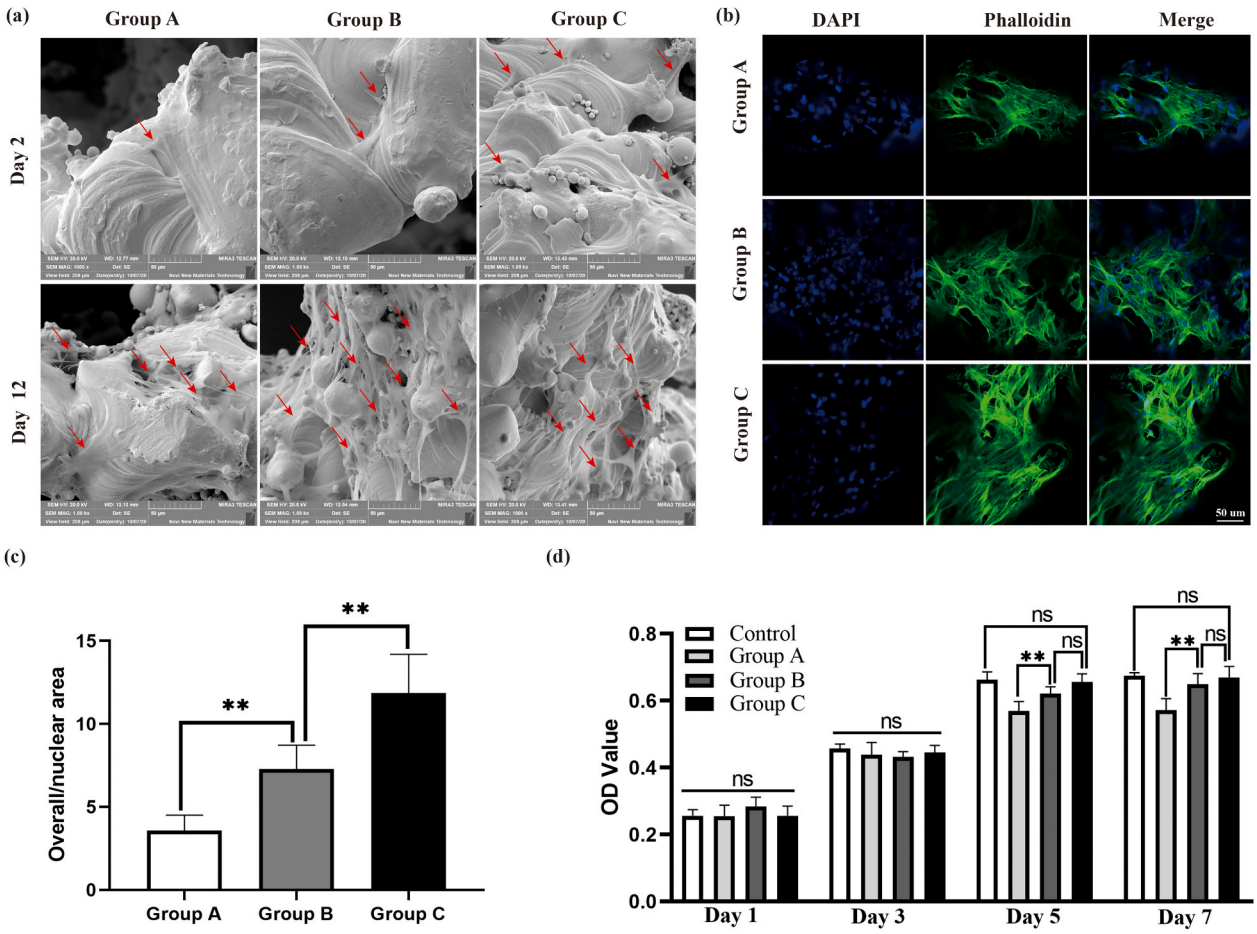

Fig. 3. Biocompatibility of the novel scaffolds. (a) Representative scanning electron microscopy (SEM) images of r-BMSCs on the scaffolds at day 2 and day 12, (b–c) DAPI/phalloidin fluorescence labeling images of r-BMSCs at day 7 and corresponding quantitative analysis of cellular area to nucleus, (d) proliferation of r-BMSCs on the scaffolds. (**P < 0.01).

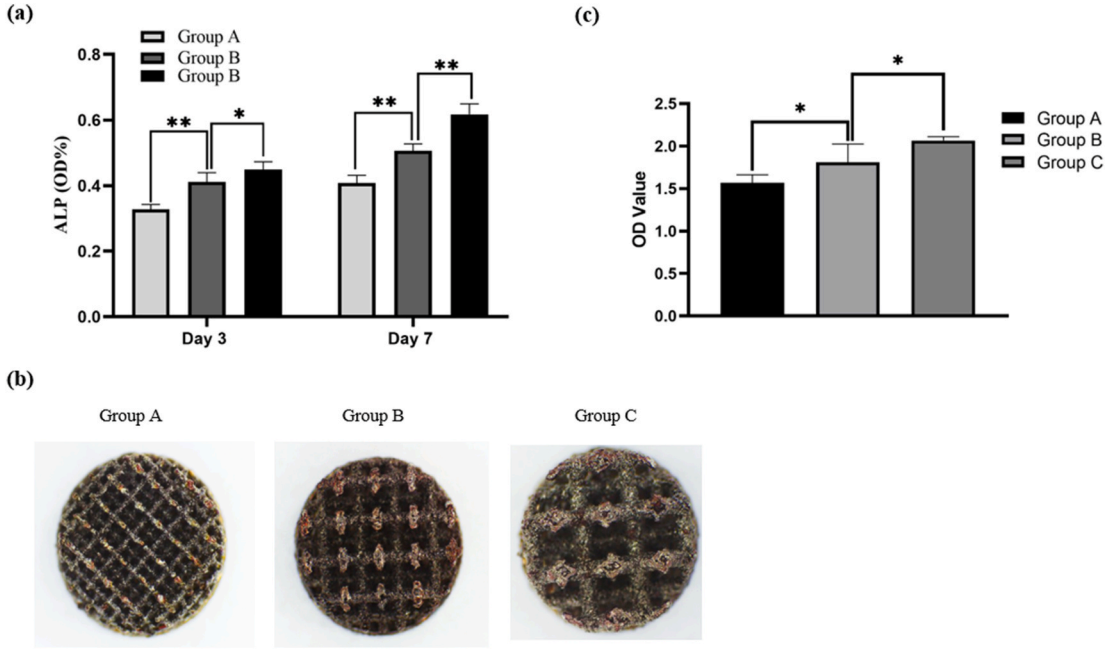

Fig. 4. In vitro osteogenesis determination. (a) Alkaline phosphatase (ALP) production generated from the r-BMSCs on the scaffolds after culturing for 3 and 7 days, (b) representative images of alizarin red staining of mineralized nodules, (c) quantitative analysis of dissolved mineralized nodules. (*P < 0.05, **P < 0.01). (For interpretation of the references to color in this figure legend, the reader is referred to the Web version of this article.)

inside the homogeneous pores of the scaffolds, and good integration between the porous scaffolds and the host bone was observed (Fig. 5a). Regarding micro-CT detection, the new bone tissue (gray) grew into the porous stents (yellow), which was observed around and inside the scaffolds and almost fully merged into the pores of the scaffolds, indicating excellent integration between the new bone and porous scaffolds (Fig. 5b). Statistical analysis showed that the BV/TV and Tb·N indexes of group C scaffolds were relatively higher than those of the other two groups, confirming the results of the 3D reconstruction images (Fig. 5c and d).

3.4.2. Histological evaluation

Finally, a histological evaluation was performed to assess the osteogenesis and osseointegration of the Ti6Al4V-based porous Ta scaffolds. Van Gieson and toluidine blue staining were employed for histological evaluation. Van Gieson staining showed that visible bone ingrowth (red) was observed not only inside the porous scaffolds but also at the interface between the substrate and porous scaffolds in each group (Fig. 6a). The beams of the scaffolds were surrounded by bone; there were tiny gaps between the new bone and the beams. A large number of bone-lining cells was observed around the beams, indicating that bone regeneration was already activated. Purple staining was also observed in some regions, indicating the presence of cartilage-like tissue. The results of toluidine blue staining were in line with those of Van Gieson staining (Fig. 6b); the beams of porous scaffolds were surrounded with new bone (blue), and bone ingrowth was also present at the interface between the substrate and porous Ta. Consistent with the staining, SEM analysis indicated that Ti6Al4V-based porous Ta scaffolds showed favorable osteointegration (Fig. 6c). To further confirm the bone ingrowth inside the porous scaffolds and explore the elementary cross-sectional distribution in the scaffolds, EDS was performed. The results showed that calcium and phosphorus were present inside the porous scaffolds, nearly bridging the cross-section (Fig. 6d), which confirmed the presence of new bone inside the scaffolds. These results revealed that the in vivo osseointegration of the Ti6Al4V-based porous Ta scaffolds was satisfactory.

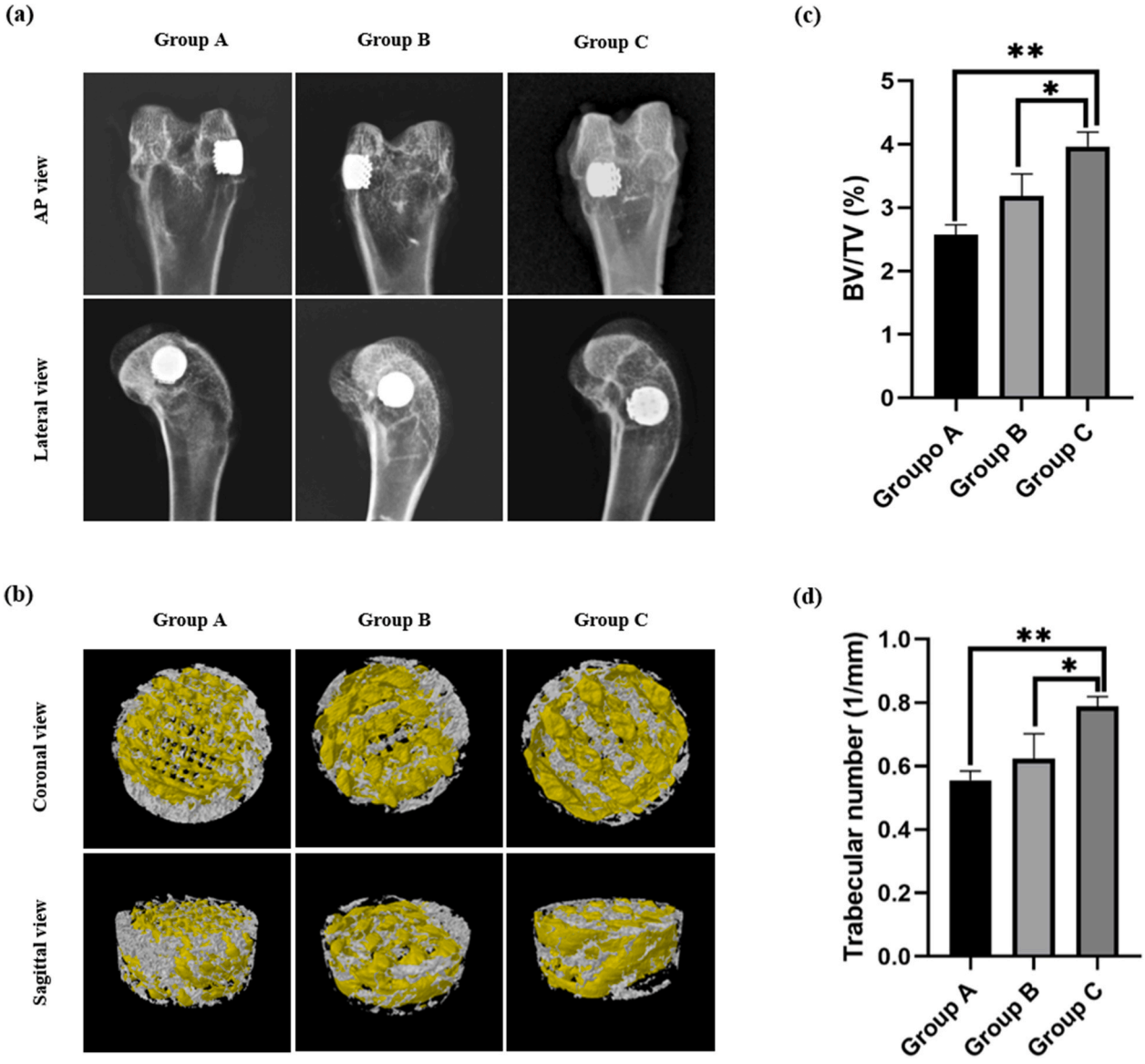

Fig. 5. Imageology analysis of the in-vivo animal experiment. (a) Representative X-ray images of the femur specimens at sixth week after implantation, (b) representative. 3D reconstructive images of Micro-CT analysis, (c–d) quantitative analysis of the ratio of bone volume to tissue volume (BV/TV) and trabecular number (Tb·N). (*$P < 0.05$, **$P < 0.01$).

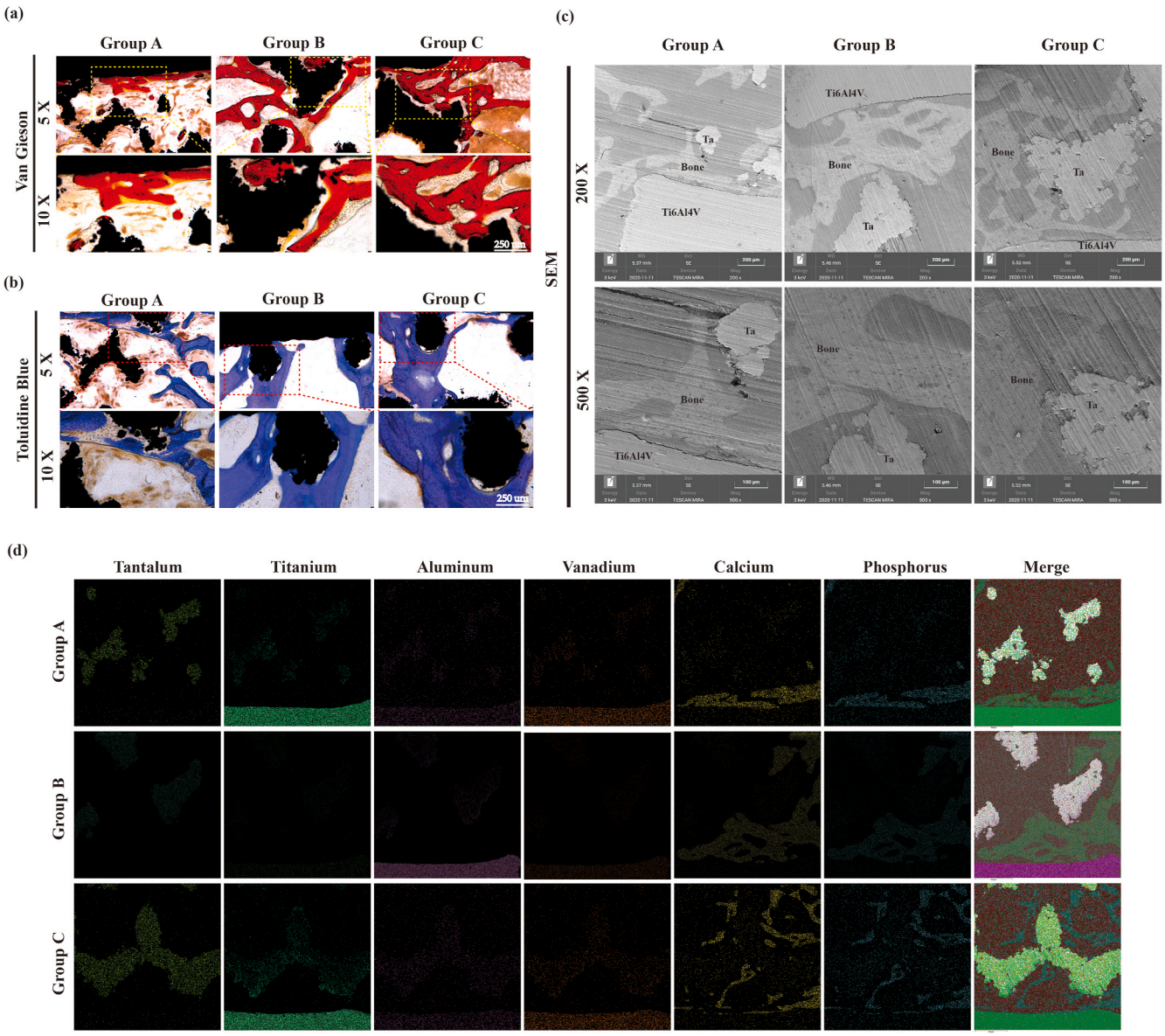

Fig. 6. Histological analysis of the in-vivo animal experiment. (a–b) Representative images of the van Geison's staing and toluidine blue staining at postoperative six weeks, (c) SEM micrographs of new bone agglomerates and bone microstructure surrounding and inside the scaffolds, (d) EDS images for screening the distribution of elements in the hard tissue sections. (For interpretation of the references to color in this figure legend, the reader is referred to the Web version of this article.)

4. Discussion

In the present study, we developed a novel high-interface-strength Ti6Al4V-based porous Ta scaffold using LPBF, in which porous Ta was additively manufactured on a solid Ti6Al4V substrate directly. The mechanical evaluation revealed that the compressive modulus and compressive strength of the novel scaffold were favorable for bone ingrowth, and the ultimate interfacial bonding strength was much higher than that of the human cortical bone. In vitro and in vivo experiments demonstrated that the biocompatibility and osteointegration were excellent. Our newly developed complex scaffold exhibits great potential for clinical orthopedic applications.

Scaffolds designed for orthopedic implantation should have good biocompatibility, osteointegration capacity, and appropriate mechanical properties that facilitate bone ingrowth [26]. Many attempts have been made to combine the advantages of Ti6Al4V (Ti) and Ta in the same scaffold [7,27–29]. However, as mentioned previously, it remains challenging to obtain both satisfactory mechanical properties and biological activity, regardless of using Ti6Al4V–Ta alloy or Ta coating on Ti6Al4V. The Ti6Al4V-Ta alloy cannot maximize the biological activity of Ta, because the cell growth on the Ti-Ta alloy is not comparable to pure Ta until the proportion of Ta is as high as 80% [11], which does not address the high cost and density of Ta. In contrast, Sing et al. reported that the compressive modulus of Ti-Ta alloy containing 50% (weight) Ta manufactured using LPBF is 75.77 ± 4.04 GPa [9], consistent with the results of Fuerst et al. (88 GPa for Ti–50Ta) [11]. This is far from what is required for the human bone tissue (0.5–20 GPa) [17], and mismatched moduli would result in "stress shielding" and subsequent premature failure of the implanted scaffolds [30]. Additionally, the controversy about the appropriate proportion of Ta in the Ti6Al4V-Ta alloy exists continuously, and it is quite difficult to obtain an optimal proportion to tailor the bioactivity and mechanical properties [9–11,13,26,27]. Regarding the Ta coating on the surface of Ti6Al4V, the principal concern was the bonding strength between the Ti6Al4V substrate and the Ta coating. Roy et al. [4,8], Dittrick et al. [31], and Balla et al. [7] achieved Ta coating on Ti substrates using laser engineered net shaping; however, the bonding strength was not expounded. Moreover, they reported a sharp interface between the porous Ta coating and the

substrate, which may have led to low fatigue resistance. To remove the sharp interface, the Ta coating can be manufactured in a dense structure [7], but then, the scaffold does not provide a porous structure for cell attachment and bone ingrowth.

Well-modified mechanical properties are the primary prerequisite for composite metallic scaffolds. The primary obligation of orthopedic scaffolds is to substitute for the non-functioning bone and provide adequate mechanical support; therefore, manufactured scaffolds should possess mechanical characteristics comparable to those of the human bone [32]. In this study, the compressive strength of the newly developed scaffolds reached over 6 MPa, which was higher than that of human cancellous bone (2–5 MPa) and sufficient for mechanical support [33,34]. Mechanical characteristics are not only crucial for load-bearing but also for biological activity, because mechanical signals can be transferred into biological signals [34,35]. Increasing evidence has demonstrated that the compressive modulus of scaffolds is significantly associated with the differentiation of stem cells [36]. BMSCs differentiate into osteoblasts when exposed to materials with compressive modulus over 25 kPa [36], and the mismatched compressive modulus is usually associated with poor osteointegration. The compressive modulus of our novel scaffolds matched well with that of the human bone tissue, which contributed to the osteogenic differentiation of r-BMSCs and averted “stress shielding”. These results confirmed that the mechanical properties of our newly developed scaffolds met the requirements of ideal implants.

As mentioned previously, sufficient bonding strength is the key for complex metal scaffolds since it is crucial for in vivo mechanical stability. Moreover, because the orthopedic scaffolds implanted into the human body were load-bearing at all times, in composite scaffolds, if the bonding strength was not strong enough, the porous structure would loosen or fall, resulting in serious complications. To achieve high interface strength between the Ti6Al4V substrate and porous Ta scaffolds, we applied LPBF and fabricated solid Ti6Al4V first, and then manufactured porous Ta directly on it, during which the closed bonding was established. According to the standard tensile adhesion test (ASTM C633) [37], we attached the glue to the surface of the porous Ta to detect the bonding strength, but observed no fissures in the scaffolds even if the glue was delaminated and torn. Therefore, flat dog-bone-shaped coupons were manufactured for interfacial bonding testing, and the results revealed that the bonding strength was much higher than that of the natural bone tissue. The results generated using EDS at the interface between Ta and the substrate could account for the high interfacial bonding strength. After the Ti6Al4V substrate was prepared, Ta powder was deposited on it and melted using a laser, during which the surface of the formed Ti6Al4V also melted because the melting point of Ta (3017 °C) is much higher than that of Ti (1650 °C), Al (660 °C), and V (1890 °C) [27]. In addition, the density of Ta was nearly four times higher than that of Ti. As a result, the melted Ta solution sank and metallurgically fused with Ti6Al4V. Moreover, the high interface strength can be further explained by the Marangoni effect. This effect indicates the flow of liquids due to the local interfacial tension difference. The intense Marangoni force led to the thermocapillary-driven transfer of mass at the heterogeneous material interface during the fabrication of novel scaffolds, in which Ta was pushed into the molten Ti6Al4V pool while liquid Ti6Al4V penetrated the upper Ta pool [38]. Therefore, it was not surprising that the interfacial bonding strength of the novel scaffold was excellent.

BMSCs are multi-lineage cells that play a pivotal role in all stages of osteogenesis, including cellular propagation and osteoblast differentiation [39]. Additionally, a myriad of evidence has demonstrated that BMSCs also secrete bioactive substances to promote osteogenesis, such as exosomes [40]. Considering the above-mentioned merits, r-BMSCs were selected for biological determinations in this study.

Biocompatibility is the most important biological performance of orthopedic scaffolds, which was assessed through cell morphology and proliferation in the present study. After seeding onto the scaffolds, r-BMSCs adhered to the surface first, and then initiated a series of biological phenomena, including cell spreading, cytoskeletal development, and proliferation [41]. We observed the cell morphology through SEM, which revealed that r-BMSCs spread out completely and connected with the neighboring cells, and interlaced cellular networks and layers were formed on the surface of the scaffolds. The cells adhered to the rugged regions of the scaffolds via cellular pseudopods, suggesting that the cells attached well [42]. Moreover, in the present study, the gap between the cells was quite small, which could facilitate well-modified signaling and substance transport among the adjoining cells [43]. In summary, SEM characterization demonstrated favorable adhesion of r-BMSCs on the scaffolds. The cytoskeleton, including microtubules, microfilaments, and intermediate filaments, are important transporters of biomolecules between the nucleus and the cytoplasm and are also pivotal for cellular shape, division, and function [44]. We labeled the nucleus and microfilaments to characterize the intracellular microstructures and observed abundant mature cytoskeletons and growing actin filaments in all three groups on day 7 after seeding onto the newly developed scaffolds, demonstrating that r-BMSCs were in a state of active metabolism. In line with the above morphological results, CCK8 assay identified no significant difference between the experimental groups and the control group regarding the proliferation rate, indicating the good biocompatibility of the cells on the scaffolds. The newly developed Ti6Al4V-based porous Ta scaffolds were biocompatible.

Osteointegration is another crucial criterion for orthopedic scaffolds [45]. A large amount of evidence derived from clinical and laboratory studies has proved the outstanding osteointegration performance of Ta [13,46], which was also demonstrated to be superior to Ti via ample studies [17,47]. Two canonical detection approaches, ALP and mineralized nodule production, were chosen to evaluate the osteogenesis performance of the newly developed scaffolds in the present study. The production of ALP is a classic indicator of early-stage osteogenesis [48]. A considerable amount of ALP was detected in each group, indicating that the newly developed scaffold was favorable for early osteogenesis. Additionally, a significant increase in ALP production was observed from day 3–7, which could be reasonably interpreted via the osteogenic differentiation of r-BMSCs. With the prolonged culture time, r-BMSCDs continued to develop to terminal osteogenic differentiation, and the production of mineralized extracellular matrix (ECM) was employed to characterize it. The mineralized ECM is produced in the later phase of osteogenic differentiation and plays an essential role in bone remodeling [49]. Alizarin red is a specialized coloring agent for mineralized nodules, and stained clusters were observed in this study, indicating well-developed bone formation. The in vitro osteogenesis performance of the newly developed scaffolds was satisfactory.

Bone regeneration is an intricate, well-orchestrated physiological process that can be influenced by many potential factors, including the osteogenic activity of scaffolds, secretion of bioactive molecules, and mechanical parameters [50,51]. In vitro osteogenesis partly reflects the osteointegration of the scaffolds, because the in vivo biological and mechanical environment is far more complex [35]. Therefore, we implanted the newly developed scaffolds into rabbits with femoral condyle defects, and imaging and histological evaluation were applied to assess osteointegration. The histological determination is a precise and direct-viewing approach for evaluating bone ingrowth [52], which displays what exists directly. Our results indicated the integration of host bone scaffolds, although there were a few crannies between the scaffolds and the new bone in the histological sections. This might be due to hard tissue cutting since we observed no gaps in the reconstructed micro-CT images. To further confirm the ingrowing bone, we used EDS, in which the dominant components of natural bone tissue, calcium and phosphorus [53], were detected as expected. These in vivo findings collectively indicate the outstanding osteointegration properties of the scaffolds.

Slight differences were identified among the three groups in our study, and group C seemed to be relatively preferable, which was

somewhat contradictory to the optimal pore size reported previously (200–500 μm) [11,54]. This might be because the porosity was the sole fixed coefficient, and the other parameters varied systematically in the present study. More cells attached to the surface of the scaffolds with larger beam size, and as a result, a preferable biological performance was observed in vitro. Six-week implantation was relatively short to demonstrate the differences among groups, and extended implantation may neutralize the deviations. Further comprehensive and longer studies need to be conducted to optimize the scaffolds, as the main focus of this study was to introduce the newly developed high interface-strength scaffold and assess its osteointegration activity. As for the specific mechanisms through which Ta scaffolds promote osteointegration, including osteogenic differentiation, osteogenesis, and osteoinduction, various hypotheses have been proposed [55]. Shi et al. demonstrated that the TGF-β/Smad signaling pathway mediates the effect of Ta on osteogenic differentiation [56]. Lu et al. reported that Ta promotes osteogenesis by triggering the BMP2/Smad1 signaling [57]. In our opinion, the osteointegration activity of porous Ta scaffolds resulted from the interaction of intrinsic bioactivity, adaptable mechanical properties, and the porous stereoscopic spatial structure. Deeper and comprehensive investigations are warranted to explore the underlying mechanisms.

Nowadays, great progress have been made in the design and analysis of Ti6Al4V lattice structures manufactured using AM [18], and personalized features could be obtained through corresponding optimization. While, in this study, we performed surface modification of Ti6Al4V using a special approach, through which porous Ta structure was constructed on the Ti6Al4V directly, making significant breakthrough in the application of Ti6Al4V. Although previous studies have demonstrated Ti-Ta alloy manufacturing and Ta coating of Ti [4,7], the concomitant drawbacks still cause great concern. In comparison to previous studies, our newly developed scaffold possesses distinct merits. First of all, the novel scaffolds combine the well-modified mechanical performance of Ti6Al4V and the favorable biological activity of Ta, at relatively low-cost with the low-priced Ti6Al4V designed as the substrate. Second, the solid Ti6Al4V substrate and porous Ta were integrated with high bonding strength through metal melting unprecedentedly, which provided a porous structure for cellular adhesion and bone ingrowth compared with solid Ta coating on Ti. Third, our novel scaffolds save a mass of materials, reduced the cost, and addressee the functional impediment derived from excessive weight compared with the Ta scaffolds fabricated on the Ta substrate. Last but not least, the newly developed scaffolds are not affected by the Ti6Al4V to Ta ratio compared with the alloy. Thus, the novel scaffolds have great potential for clinical application.

There were some limitations to our study. First, we evaluated the in vivo osteointegration of the novel scaffolds at a single time point (6 weeks), which was not sufficient to assess the increase in bone ingrowth over time. Second, in vivo mechanical evaluations, such as push-out testing, were not conducted to determine the bond strength between the scaffold and ambient bone tissue. Finally, although the compressive moduli were assessed, most deformation occurred in the porous Ta but not evenly distributed throughout the scaffolds, demonstrating the accurate moduli only partly.

5. Conclusion

In this study, a high-interface-strength Ti6Al4V-based porous Ta scaffold was additively manufactured using LPBF for the first time. Our results demonstrated that the newly developed scaffold is mechanically compatible, and it is favorable for r-BMSC adhesion, proliferation, and differentiation toward osteoblasts. In vivo evaluation confirmed that the scaffolds integrate well with the host bone. Altogether, these results indicate that the novel scaffold is adaptable for orthopedic implantation and possesses great potential for clinical applications. Further studies are needed to optimize scaffolds and elucidate the underlying biological mechanisms.

CRediT authorship contribution statement

Pengfei Lei: Investigation, Data curation, Writing – original draft, Methodology, Software. **Hu Qian:** Investigation, Data curation, Writing – original draft, Methodology, Software. **Taomei Zhang:** Visualization, Investigation, Methodology. **Ting Lei:** Investigation, Formal analysis, Methodology. **Yihe Hu:** Conceptualization, Project administration, Funding acquisition, Supervision. **Chao Chen:** Conceptualization, Project administration, Writing – review & editing. **Kechao Zhou:** Supervision, Project administration.

Declaration of competing interest

The authors declare that they have no conflicts of interest.

Acknowledgments

This study was supported by the Natural Science Foundation of Hunan Province, China (Grant No. 2019JJ40499), the Scientific Research Project of Health and Family Planning Commission of Hunan Province, China (Grant No. B2019188), the Science and technology Innovation Leading Project for High-tech Industry of Hunan Province (Grant No. 2020SK2008), the Major science and technology projects of Changsha City (Grant No. 42193), National key research and development project (2018YFB1105504), Natural Science Foundation of China (Grant No. 82002277 and 81672656).Thank the Teacher Zhang plotting for preparation of pictures.

References

[1] A.A. Zadpoor, Meta-biomaterials, Biomater. Sci. 8 (2019) 18–38.
[2] M. Kaur, K. Singh, Review on titanium and titanium based alloys as biomaterials for orthopaedic applications, Materials science & engineering C, Materials for biological applications 102 (2019) 844–862.
[3] R. Wauthle, S.M. Ahmadi, S. Amin Yavari, et al., Revival of pure titanium for dynamically loaded porous implants using additive manufacturing, Materials science & engineering C, Materials for biological applications 54 (2015) 94–100.
[4] M. Roy, V.K. Balla, A. Bandyopadhyay, et al., MgO-doped tantalum coating on Ti: microstructural study and biocompatibility evaluation, ACS Appl. Mater. Interfaces 4 (2012) 577–580.
[5] Q. Han, C. Wang, H. Chen, et al., Porous tantalum and titanium in orthopedics: a review, ACS Biomater. Sci. Eng. 5 (2019) 5798–5824.
[6] S.P. Russell, C.J. O'Neill, E.J. Fahey, et al., Trabecular metal augments for severe acetabular defects in revision hip arthroplasty: a long-term follow-up, J. Arthroplasty 36 (5) (2021) 1740–1745.
[7] V.K. Balla, S. Banerjee, S. Bose, et al., Direct laser processing of a tantalum coating on titanium for bone replacement structures, Acta Biomater. 6 (2010) 2329–2334.
[8] M. Roy, V.K. Balla, S. Bose, et al., Comparison of tantalum and hydroxyapatite coatings on titanium for applications in load bearing implants, Adv. Eng. Mater. 12 (2010) B637–B641.
[9] S.L. Sing, F.E. Wiria, W.Y. Yeong, Selective laser melting of titanium alloy with 50 wt% tantalum: effect of laser process parameters on part quality, Int. J. Refract. Metals Hard Mater. 77 (2018) 120–127.
[10] N. Soro, H. Attar, E. Brodie, et al., Evaluation of the mechanical compatibility of additively manufactured porous Ti-25Ta alloy for load-bearing implant applications, Journal of the mechanical behavior of biomedical materials 97 (2019) 149–158.
[11] J. Fuerst, D. Medlin, M. Carter, et al., LASER additive manufacturing of titanium-tantalum alloy structured interfaces for modular orthopedic devices, JOM (J. Occup. Med.) 67 (2015) 775–780.
[12] L. Yan, Y. Yuan, L. Ouyang, et al., Improved mechanical properties of the new Ti-15Ta-xZr alloys fabricated by selective laser melting for biomedical application, J. Alloys Compd. 688 (2016) 156–162.
[13] S. Huang, S.L. Sing, G. de Looze, et al., Laser powder bed fusion of titanium-tantalum alloys: compositions and designs for biomedical applications, Journal of the mechanical behavior of biomedical materials 108 (2020), 103775.
[14] Y. Katsuura, S.A. Qureshi, Additive manufacturing for metal applications in orthopaedic surgery, J. Am. Acad. Orthop. Surg. 28 (2020) e349–e355.
[15] R. Wauthle, J. van der Stok, S. Amin Yavari, et al., Additively manufactured porous tantalum implants, Acta Biomater. 14 (2015) 217–225.
[16] R. Gao, Y. Xiong, H. Zhang, et al., Mechanical properties and biocompatibilities of radially graded porous titanium/tantalum fabricated by selective laser melting, Rare Met. Mater. Eng. 50 (2021) 249–254.

[17] Y. Guo, K. Xie, W. Jiang, et al., In vitro and in vivo study of 3D-printed porous tantalum scaffolds for repairing bone defects, ACS Biomater. Sci. Eng. 5 (2019) 1123–1133.
[18] S. Maietta, A. Gloria, G. Improta, et al., A further analysis on Ti6Al4V lattice structures manufactured by selective laser melting, Journal of healthcare engineering 2019 (2019), 3212594.
[19] A. Razavykia, E. Brusa, C. Delprete, et al., An overview of additive manufacturing technologies-A review to technical synthesis in numerical study of selective laser melting, Materials 13 (2020).
[20] A. Falkowska, A. Seweryn, M. Skrodzki, Strength properties of a porous titanium alloy Ti6Al4V with diamond structure obtained by laser power bed fusion (LPBF), Materials 13 (2020).
[21] K. Song, M. Huang, Q. Shi, et al., Cultivation and identification of rat bone marrow-derived mesenchymal stem cells, Mol. Med. Rep. 10 (2014) 755–760.
[22] T. Lei, H. Qian, P. Lei, et al., The increased oxygen content in tantalum leads to decreased bioactivity and osteogenic ability of tantalum implants, Biomater. Sci. 9 (2021) 1409–1420.
[23] L. Jiang, W. Zhang, L. Wei, et al., Early effects of parathyroid hormone on vascularized bone regeneration and implant osseointegration in aged rats, Biomaterials 179 (2018) 15–28.
[24] A. Bandyopadhyay, I. Mitra, A. Shivaram, et al., Direct comparison of additively manufactured porous titanium and tantalum implants towards in vivo osseointegration, Addit Manuf 28 (2019) 259–266.
[25] R. Havaldar, S.C. Pilli, B.B. Putti, Insights into the effects of tensile and compressive loadings on human femur bone, Adv. Biomed. Res. 3 (2014) 101.
[26] H. Qian, T. Lei, P. Lei, et al., Additively Manufactured Tantalum Implants for Repairing Bone Defects: a Systematic Review, Tissue Eng. B Rev. 27 (2) (2021) 166–180.
[27] S.L. Sing, W.Y. Yeong, F.E. Wiria, Selective laser melting of titanium alloy with 50 wt% tantalum: microstructure and mechanical properties, J. Alloys Compd. 660 (2016) 461–470.
[28] Q. Huang, S. Xu, Z. Ouyang, et al., Multi-scale nacre-inspired lamella-structured Ti-Ta composites with high strength and low modulus for load-bearing orthopedic and dental applications, Materials science & engineering C, Materials for biological applications 118 (2021), 111458.
[29] P. Fox, S. Pogson, C.J. Sutcliffe, et al., Interface interactions between porous titanium/tantalum coatings, produced by Selective Laser Melting (SLM), on a cobalt-chromium alloy, Surf. Coating. Technol. 202 (2008) 5001–5007.
[30] L.E. Murr, Open-cellular metal implant design and fabrication for biomechanical compatibility with bone using electron beam melting, Journal of the mechanical behavior of biomedical materials 76 (2017) 164–177.
[31] S. Dittrick, V.K. Balla, S. Bose, et al., Wear performance of laser processed tantalum coatings, Materials Science & Engineering C-Materials for Biological Applications 31 (2011) 1832–1835.
[32] S. Miramini, K.L. Fegan, N.C. Green, et al., The status and challenges of replicating the mechanical properties of connective tissues using additive manufacturing, Journal of the mechanical behavior of biomedical materials 103 (2020), 103544.
[33] L. Polo-Corrales, M. Latorre-Esteves, J.E. Ramirez-Vick, Scaffold design for bone regeneration, J. Nanosci. Nanotechnol. 14 (2014) 15–56.
[34] J.L. Allen, M.E. Cooke, T. Alliston, ECM stiffness primes the TGFβ pathway to promote chondrocyte differentiation, Mol. Biol. Cell 23 (2012) 3731–3742.
[35] L. Geris, K. Vandamme, I. Naert, et al., Mechanical loading affects angiogenesis and osteogenesis in an in vivo bone chamber: a modeling study, Tissue Eng. 16 (2010) 3353–3361.
[36] A.J. Engler, S. Sen, H.L. Sweeney, et al., Matrix elasticity directs stem cell lineage specification, Cell 126 (2006) 677–689.
[37] Y.C. Yang, E. Chang, Influence of residual stress on bonding strength and fracture of plasma-sprayed hydroxyapatite coatings on Ti-6Al-4V substrate, Biomaterials 22 (2001) 1827–1836.
[38] C.L. Tan, K.S. Zhou, W.Y. Ma, et al., Interfacial characteristic and mechanical performance of maraging steel-copper functional bimetal produced by selective laser melting based hybrid manufacture, Mater. Des. 155 (2018) 77–85.
[39] S.C. Chuang, C.H. Chen, Y.S. Chou, et al., Protein-coupled estrogen receptor mediates cell proliferation through the cAMP/PKA/CREB pathway in murine bone marrow mesenchymal stem cells, Int. J. Mol. Sci. (2020) 21.
[40] G.D. Lu, P. Cheng, T. Liu, et al., BMSC-derived exosomal miR-29a promotes angiogenesis and osteogenesis, Frontiers in cell and developmental biology 8 (2020), 608521.
[41] D.G. Castner, B.D. Ratner, Biomedical surface science: foundations to frontiers, Surf. Sci. 500 (2002) 28–60.
[42] C. Wu, Y. Zhang, Y. Zhu, et al., Structure-property relationships of silk-modified mesoporous bioglass scaffolds, Biomaterials 31 (2010) 3429–3438.
[43] K. Matsuo, N. Irie, Osteoclast-osteoblast communication, Arch. Biochem. Biophys. 473 (2008) 201–209.
[44] K.G. B W, The evolution of the cytoskeleton, J. Cell Biol. 194 (4) (2011 Aug 22) 513–525.
[45] B.G. Zhang, D.E. Myers, G.G. Wallace, et al., Bioactive coatings for orthopaedic implants-recent trends in development of implant coatings, Int. J. Mol. Sci. 15 (2014) 11878–11921.
[46] B.R. Levine, S. Sporer, R.A. Poggie, et al., Experimental and clinical performance of porous tantalum in orthopedic surgery, Biomaterials 27 (2006) 4671–4681.
[47] S. Piglionico, J. Bousquet, N. Fatima, et al., Porous tantalum VS. Titanium implants: enhanced mineralized matrix formation after stem cells proliferation and differentiation, J. Clin. Med. 9 (2020).
[48] M.F. Pittenger, A.M. Mackay, S.C. Beck, et al., Multilineage potential of adult human mesenchymal stem cells, Sci. (N. Y.) 284 (1999) 143–147.
[49] A.I. Alford, K.M. Kozloff, K.D. Hankenson, Extracellular matrix networks in bone remodeling, Int. J. Biochem. Cell Biol. 65 (2015) 20–31.
[50] R. Dimitriou, E. Jones, D. McGonagle, et al., Bone regeneration: current concepts and future directions, BMC Med. 9 (2011) 66.
[51] A. Ho-Shui-Ling, J. Bolander, L.E. Rustom, et al., Bone regeneration strategies: engineered scaffolds, bioactive molecules and stem cells current stage and future perspectives, Biomaterials 180 (2018) 143–162.
[52] K.D. Draenert, Y.I. Draenert, R. Krauspe, et al., Strain adaptive bone remodelling in total joint replacement, Clin. Orthop. Relat. Res. (2005) 12–27.
[53] J.J. Anderson, Calcium, phosphorus and human bone development, J. Nutr. 126 (1996) 1153s–1158s.
[54] N. Taniguchi, S. Fujibayashi, M. Takemoto, et al., Effect of pore size on bone ingrowth into porous titanium implants fabricated by additive manufacturing: an in vivo experiment, Materials science & engineering C, Materials for biological applications 59 (2016) 690–701.
[55] H. Qian, T. Lei, Z. Ye, et al., From the performance to the essence: the biological mechanisms of how tantalum contributes to osteogenesis, BioMed Res. Int. 2020 (2020), 5162524.
[56] L.Y. Shi, A. Wang, F.Z. Zang, et al., Tantalum-coated pedicle screws enhance implant integration, Colloids Surf. B Biointerfaces 160 (2017) 22–32.
[57] M.M. Lu, P.S. Wu, X.J. Guo, et al., Osteoinductive effects of tantalum and titanium on bone mesenchymal stromal cells and bone formation in ovariectomized rats, Eur. Rev. Med. Pharmacol. Sci. 22 (2018) 7087–7104.